ADVANCED MATERIALS
www.advmat.de

Microstructured Hydrogels to Guide Self-Assembly and Function of Lung Alveolospheres

Claudia Loebel, Aaron I. Weiner, Madeline K. Eiken, Jeremy B. Katzen, Michael P. Morley, Vikram Bala, Fabian L. Cardenas-Diaz, Matthew D. Davidson, Kazushige Shiraishi, Maria C. Basil, Laura T. Ferguson, Jason R. Spence, Matthias Ochs, Michael F. Beers, Edward E. Morrisey, Andrew E. Vaughan, and Jason A. Burdick**

Epithelial cell organoids have increased opportunities to probe questions on tissue development and disease in vitro and for therapeutic cell transplantation. Despite their potential, current protocols to grow these organoids almost exclusively depend on culture within 3D Matrigel, which limits defined culture conditions, introduces animal components, and results in heterogenous organoids (i.e., shape, size, composition). Here, a method is described that relies on hyaluronic acid hydrogels for the generation and expansion of lung alveolar organoids (alveolospheres). Using synthetic hydrogels with defined chemical and physical properties, human-induced pluripotent stem cell (iPSC)-derived alveolar type 2 cells (iAT2s) self-assemble into alveolospheres and propagate in Matrigel-free conditions. By engineering predefined microcavities within these hydrogels, the heterogeneity of alveolosphere size and structure is reduced when compared to 3D culture, while maintaining the alveolar type 2 cell fate of human iAT2-derived progenitor cells. This hydrogel system is a facile and accessible system for the culture of iPSC-derived lung progenitors and the method can be expanded to the culture of primary mouse tissue derived AT2 and other epithelial progenitor and stem cell aggregates.

1. Introduction

Organoids have received considerable attention for modeling organogenesis and disease, facilitating the large screening of therapeutic molecules (e.g., proteins, drugs), and for the sourcing of cells for therapeutic transplantation.[1] With regards to the lung, organoids have primarily been applied to address questions in pulmonary biology, such as reparative mechanisms of lung progenitors and their responsiveness to regenerative and therapeutic molecules.[2] Given the importance of gas-exchange as the most fundamental function of the lungs, alveolar organoids (i.e., alveolospheres) are becoming an indispensable tool for in vitro studies, including for the modeling of distal lung injuries such as SARS-CoV-2 infections.[3] The alveolar epithelium comprises two distinct epithelial

C. Loebel
Department of Materials Science & Engineering
University of Michigan
North Campus Research Complex, 2800 Plymouth Rd
Ann Arbor, MI 48109, USA
E-mail: loebelcl@umich.edu

C. Loebel, M. K. Eiken, V. Bala, J. R. Spence
Department of Biomedical Engineering
University of Michigan
Carl A. Gerstacker Building, 2200 Bonisteel Blvd
Ann Arbor, MI 48109, USA

C. Loebel, M. D. Davidson, J. A. Burdick
Department of Bioengineering
University of Pennsylvania
240 Skirkanich Hall 210 S. 33rd Street, Philadelphia, PA 19104, USA

A. I. Weiner, J. B. Katzen, M. P. Morley, F. L. Cardenas-Diaz, K. Shiraishi, M. C. Basil, L. T. Ferguson, M. F. Beers, E. E. Morrisey, A. E. Vaughan
Department of Medicine
Lung Biology Institute
University of Pennsylvania
3450 Hamilton Walk, Stemmler Hall, Philadelphia, PA 19104, USA

The ORCID identification number(s) for the author(s) of this article can be found under https://doi.org/10.1002/adma.202202992.

DOI: 10.1002/adma.202202992

M. D. Davidson, J. A. Burdick
BioFrontiers Institute and Department of Chemical and Biological Engineering
University of Colorado Boulder
3415 Colorado Avenue, 596 UCB, Boulder, CO 80309, USA
E-mail: jason.burdick@colorado.edu

J. R. Spence
Department of Internal Medicine – Gastroenterology
University of Michigan
109 Zina Pitcher Place, Ann Arbor, MI 48109, USA

M. Ochs
Institute of Functional Anatomy
Charité – Universitätsmedizin Berlin
Campus Charité Mitte, Philippstraße 12, 10115 Berlin, Germany

A. E. Vaughan
School of Veterinary Medicine
University of Pennsylvania
3800 Spruce St, Philadelphia, PA 19104, USA

cell types: Type 2 cells (AT2), which are surfactant-producing alveolar progenitor cells that can self-renew and differentiate into type 1 cells (AT1) that cover the majority of the surface of the lung alveoli.[4] When cultured in Matrigel and with mesenchymal feeder cells, primary mouse-derived AT2 cells form alveolospheres that comprise both AT1 and AT2 cells but often do not reproduce the structure of alveoli in adult lungs.[2] Importantly, recent advances in the differentiation of induced pluripotent stem cells (iPSCs) into AT2 cells have also enabled the culture of human alveolospheres, overcoming some of the challenges in the isolation and culture of primary human AT2 cells.[5]

Although the spontaneous assembly and propagation of organoids within Matrigel have resulted in significant advances, artificial niches are increasingly being developed to provide distinct chemical and physical signals to organoids during culture.[6] Specifically, synthetic niches can guide cellular self-assembly while overcoming challenges in Matrigel organoid cultures, such as the inherent variability in organoid formation efficiencies and morphology, which poses issues for standardizing organoid models across laboratories with quantitative readouts.[1,7] Several engineering modalities such as customized synthetic hydrogels,[8] bioprinting[9] and microfluidics[10] have been implemented to increase the number of controllable parameters during organoid cultures, such as cell–matrix interactions, the organization of multiple cell types, and fluid flow. Recent efforts have also focused on matrix-free approaches, including the design of polymeric substrates with cavities to provide geometrical constraints for the generation of intestinal and pancreatic organoids.[11–13] However, little is known of how geometrical cues of matrix-free culture conditions might guide the generation and function of lung alveolospheres.

Here, we propose hydrogel culture systems as methods to form and expand lung alveolospheres. First, encapsulation within 3D hydrogels was pursued with synthetic hyaluronic acid (HA) hydrogels, which allowed for alveolosphere formation and growth when modified with laminin/entactin, but with similar heterogeneity to Matrigel controls. As an alternative, a microstructured hydrogel was developed to guide lung alveolosphere formation within microwells under Matrigel-free culture conditions. Building upon recent advances in the design of defined matrices for organoids, our approach uses synthetic HA hydrogels that are engineered to contain predefined microcavities to generate lung alveolospheres with uniform sizes within individual microwells. Control of the initial aggregate size through cell seeding densities and microwell size enabled us to explore the role of culture constraints on alveolosphere growth and maturation. Using this method, we generated human iPSC-derived alveolospheres that display AT2 functional capacities, such as expression and processing of surfactant proteins. Alveolospheres were also generated from primary mouse alveolar progenitors, providing a minimally engineered and Matrigel-free approach for guided lung organoid culture.

2. Defined 3D Hydrogels Enable SFTPC^{GFP+} Alveolosphere Formation

To illustrate the potential of hydrogels to enable assembly of alveolosphere organoids, we first employed human iPSC-derived alveolar progenitor cells (iAT2s) with a GFP knock-in cassette in one allele of the SFTPC gene, a specific marker for AT2 cells (**Figure 1**A).[14] Using a recently developed protocol,[5,15] we differentiated iPSCs (RUES2 line) into foregut endoderm followed by sorting for NKX2.1+ putative lung primordial lung progenitors and consecutive enrichment for SFTPC^{GFP+} cells (Figure 1A). The differentiation protocol resulted in a total yield of ≈55% SFTPC^{GFP+} cells on day 66 in Matrigel (Figure 1B). The resulting SFTPC^{GFP+} cells were further purified and passaged as alveolospheres in the presence of lung maturation additives and selective Rho-associated kinase (ROCK) inhibitor, Y-27632 from days 0 to 2. CHIR was added back following 7 days of withdrawal (days 2–9) to increase efficiency of iAT2 maturation[5] (Figure 1C). Thus, this protocol allows for iAT2 serial passaging upon dissociation into single cells and formation of alveolospheres that retain SFTPC^{GFP+} expression in Matrigel.

To demonstrate alveolosphere formation in synthetic hydrogels, iAT2s were embedded within HA hydrogels (norbornene-modified HA, modified with cell-adhesive peptide (HA *RGD*), 5% Matrigel (HA *MA*), or 2 mg mL^{-1} laminin/entactin (HA *Lm*), all with a storage modulus of ≈500 Pa (Figure 1D)). At 14 days, small alveolospheres were observed in the HA *RGD* hydrogel, whereas culture in HA *MA* and HA *Lm* hydrogels resulted in increased formation of alveolospheres; however, the area was lower than Matrigel controls (Figure 1E). Alveolosphere formation further depended on the concentration of Matrigel and laminin/entactin, initial storage modulus, and iAT2 seeding density (Figure S1, Supporting Information), indicating that the formation of alveolospheres is influenced by both chemical and mechanical signals.

Alveolospheres formed within HA *Lm* hydrogels and expressed SFTPC^{GFP+} (Figure 1F), with a colony forming efficiency that was similar to Matrigel (Figure S2, Supporting Information). Furthermore, quantification of SFTPC^{GFP+} expression confirmed that alveolospheres maintain their AT2 progeny with an average of ≈31% SFTPC^{GFP+} cells (Figure 1G). Given that HA *Lm* hydrogels support alveolosphere growth, we next assessed whether iAT2s retain proliferative potential during serial passaging, consistent with previous protocols in Matrigel,[15] but using a modified enzymatic digestion (1 mg mL^{-1} hyaluronidase, no dispase). Using hyaluronidase digestion and subsequent trypsin digestion into single cell suspensions, over a period of three passages, iAT2s reformed spheres (Figure S3, Supporting Information) with stable efficiency and proliferation kinetics (Figure 1H). These findings indicate that iAT2-derived alveolospheres can be formed and maintained in laminin/entactin-enriched synthetic hydrogels, enabling culture in a well-defined Matrigel-free 3D environment. However, this strategy presents relatively high heterogeneity, because alveolospheres form randomly, similar to traditional Matrigel culture. Thus, although well-defined HA hydrogels improve culture conditions, limited control over size and shape and difficulties of standardizing toward downstream analysis remain to be addressed.

3. Design of Microwell Hydrogels for Generation of Alveolospheres

Given that iAT2s were able to form alveolospheres within a Matrigel-free hydrogel, we next sought to further control the

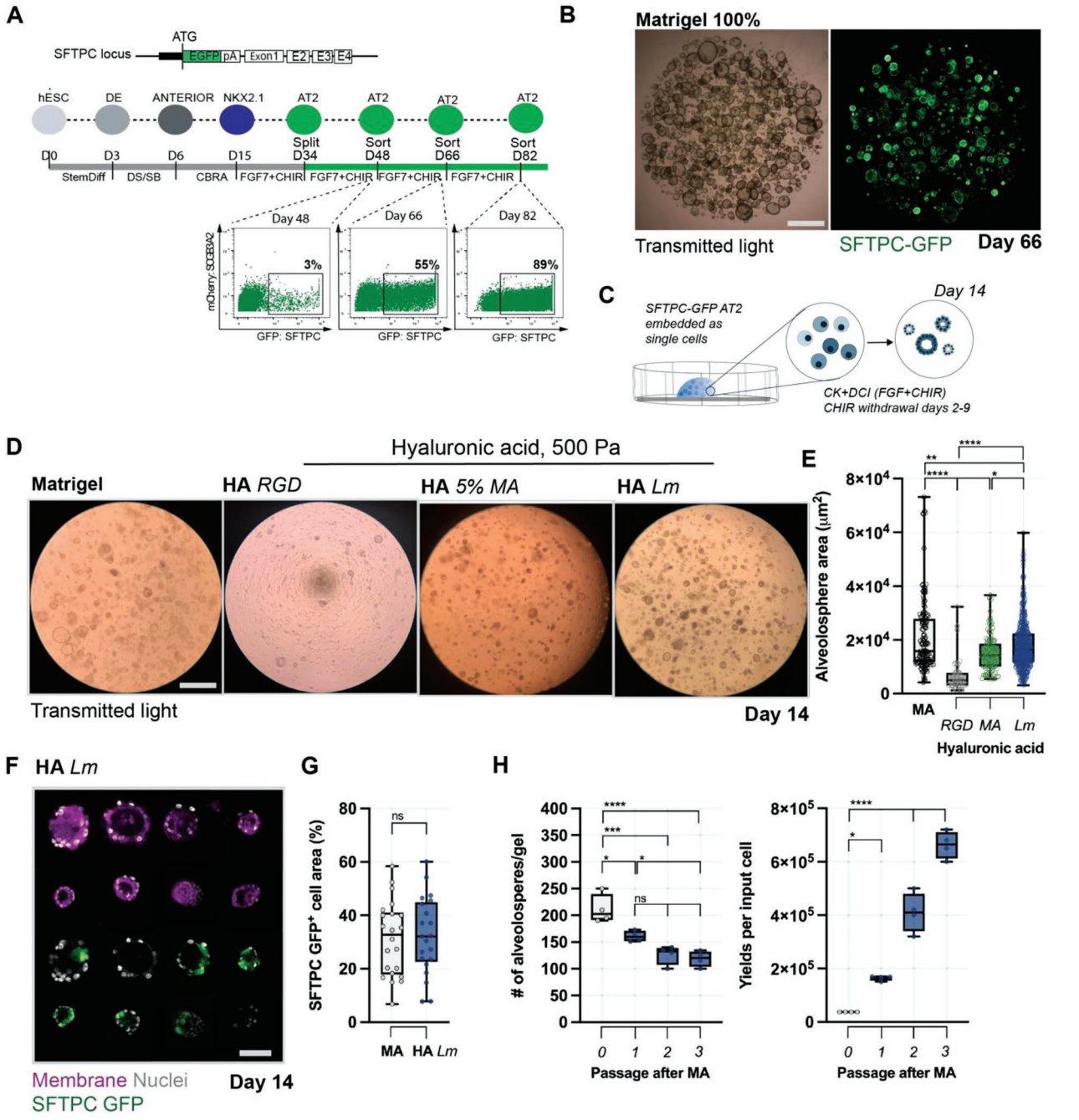

Figure 1. Tailored 3D hydrogel matrices for alveolosphere assembly and growth. A) Edited SFTPC^{GFP+} loci post Cre-mediated antibiotic cassette excision and differentiation protocol from human ESCs (RUES2) to putative iAT2s with representative flow cytometry and enrichment of GFP$^+$ cells used for subsequent studies. B) Representative images of alveolospheres showing expression of SFTPC^{GFP+} at day 66 upon GFP$^+$ enrichment and culture in Matrigel (scale bar: 100 μm). C) Schematic showing SFTPC^{GFP+} cells embedded into 3D hydrogels as a single cell suspension with 500 cells per μL and cultured with CHIR withdrawal between days 3 and 8 and CHIR addback (days 9–14). D) Representative images of alveolospheres formed in Matrigel and HA hydrogels at 14 days. HA hydrogels were crosslinked with a protease-sensitive crosslinker via visible-light-initiated thiol–ene reaction either modified with a cell-adhesive peptide (1×10^{-3} M RGD), supplemented with 5%, wt/vol Matrigel, or 2 mg mL^{-1} laminin/entactin and with crosslinker amount adjusted to achieve an initial storage (elastic) modulus of 500 Pa (scale bar: 100 μm, see Figure S1, Supporting Information, for representative images and quantification of viability and projected alveolosphere area in HA hydrogels supplemented with various concentrations of Matrigel, laminin/entactin, and the influence of elastic modulus and cell seeding density). E) Quantification of projected alveolosphere area at 14 days measured from bright-field images (*$p < 0.05$, ****$p < 0.0001$ by ANOVA and Bonferroni's multiple comparisons test, $n = 155$ (Matrigel), $n = 55$ (HA RGD), $n = 106$ (HA Ma), and $n = 154$ (HA Lm)). F) Representative images of SFTPC^{GFP+} alveolospheres in HA LM hydrogels at 14 days (cell mask membrane stain (magenta), nuclei (gray), and SFTPC^{GFP+} expression (green), scale bar: 100 μm). G) Quantification of SFTPC^{GFP+} per alveolosphere area (cell membrane stain) at 14 days (ns = not significantly different by unpaired two-tailed t-test). H) Quantification of the number of alveolospheres and proliferation kinetics of cell yield per re-embedded SFTPC^{GFP+} cells in HA Lm hydrogels over three passages.

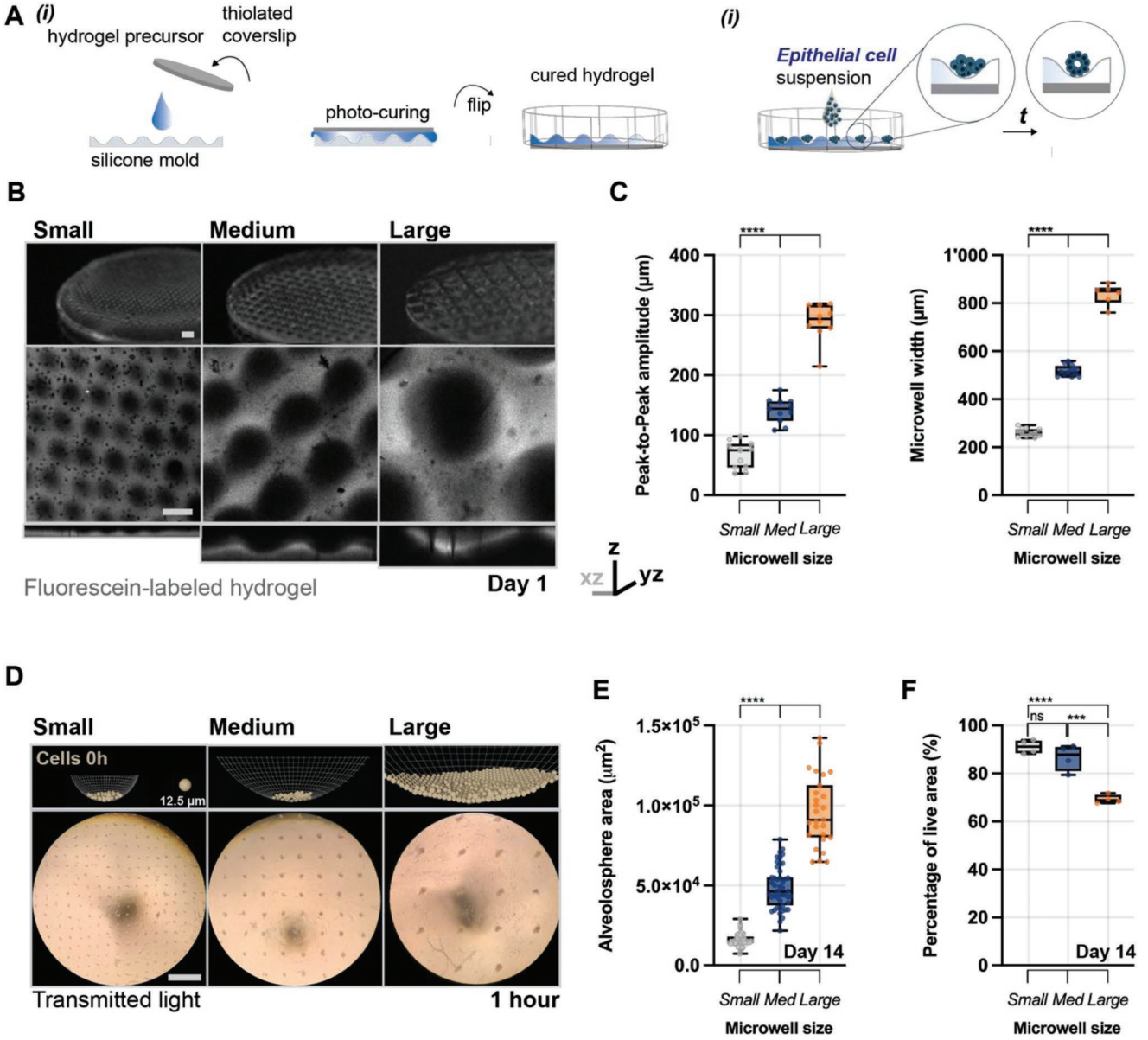

Figure 2. Design and characterization of microwell hydrogels for alveolosphere culture. A) Schematic illustrating the fabrication of microwell hydrogels: i) Silicone molds were generated by molding EZSPHERE microwell-shaped culture dishes. The microwells were then imprinted onto hydrogel surfaces during UV-light-initiated crosslinking of a norbornene-modified HA hydrogel precursor solution. ii) Single cells were seeded on top of the microwells in CD+CKI media and left to settle and form alveolospheres within individual microwells. B) Representative images of microwell HA hydrogels modified with fluorescein and fabricated from silicone molds with different widths and depths upon 1 day of swelling in saline (small: 200 µm/100 µm, medium (Med): 500 µm/200 µm, large: 800 µm/300 µm (width/depth), scale bar: 500 µm). C) Quantification of peak-to-peak amplitude and width of individual microwells upon 1 day of swelling in saline (****$p < 0.0001$ by ANOVA and Bonferroni's multiple comparisons test, $n = 11$ (small, med) and $n = 10$ (large), see Figure S5, Supporting Information, for quantifications up to day 14). D) Simulation of iAT2 cell localization upon seeding (cross-section of center of microwell) and representative images of iAT2s (≈2 cells µm^{-2}) seeded into microwells of different sizes at 1 h (cell scale 12.5 µm (simulation) and scale bar: 1 mm (microwells). E) Quantification of projected alveolosphere areas at 14 days in culture (****$p < 0.0001$ by ANOVA and Bonferroni's multiple comparisons test, $n = 27$ (small), 47 (med), 41 (large)). F) Quantification of percentage of live area (quantified by Calcein AM (live cells) and Ethidium homodimer (dead cells) staining) at 14 days in culture (****$p < 0.0001$, ***$p < 0.001$, ns = not significantly different by ANOVA and Bonferroni's multiple comparisons test, averaged from four independent experiments).

growth and homogeneity of formed alveolospheres, a critical requirement for downstream read-outs. Thus, we engineered hydrogel substrates that comprise microwell-shaped cavities for aggregation and individual alveolosphere formation through geometrical constraints (**Figure 2**). Accessibility and customization of such engineered systems is often the bottleneck for broader applications within the regenerative biology community. Here, we used commercially available cell culture surfaces (EZSPHERE) with evenly spaced microwells to make silicone replica molds of a desired size and shape (Figure S4,

Supporting Information). HA hydrogels were then fabricated with the silicone molds upon UV light-mediated photocuring onto a glass coverslip (Figure 2A-i) and subsequent transfer of the fabricated microwell hydrogels directly onto conventional tissue culture dishes (Figure 2A-ii). Using this fabrication technique, hydrogels can be readily fabricated and are compatible with a range of different sizes as shown by fluorescent images of individual microwells (Figure 2B). As the microwell size can be accurately modulated, we fabricated hydrogels (≈20 kPa) of small, medium, and large microwell sizes, ranging from an average of 80–300 μm in depth (amplitude) and 250–810 μm in width (Figure 2C). Hydrogel structures were stable during 14 days in culture in alveolosphere media with minimal changes in amplitude, width, and perimeter of individual microwells (Figure S5, Supporting Information). In addition, the initial elastic modulus of microwell hydrogels can be modulated by changing the crosslinker concentration to yield softer or stiffer hydrogels with minimal changes to microwell fidelity upon swelling (Figure S6, Supporting Information). Although several other shapes may be engineered (e.g., hexagonal or cylindrical), cell culture surfaces such as EZSPHERE that are commercially available and of various depth and width, represent a broadly applicable and generalizable culture system.

To test whether the hydrogel microwells support alveolosphere formation, we seeded iAT2s with an average density of 2 cells μm^{-2} hydrogel surface area in alveolosphere media. 3D renderings of predicted cell sedimentation into individual microwells and bright-field imaging confirmed the formation of differently sized and irregularly shaped aggregates within 1 h upon seeding, with an average of 73 ± 9% viable cells (Figure 2D). Formation of alveolospheres was controlled by the microwell size and initial seeding density, as measured by the projected alveolosphere area and viability. Within 14 days, iAT2 aggregates gave rise to alveolospheres across all microwell hydrogels (Figure S7, Supporting Information) and alveolosphere area depended on microwell size (Figure 2E). Although the efficiency and area increased in large microwells, alveolospheres also showed significantly reduced cell viability (≈70%, Figure 2F), with dead cells mostly located in the core of individual alveolospheres (Figure S8, Supporting Information), suggesting that insufficient diffusion and nutrient supply limit iAT2 survival. These results indicate that the medium-size microwell culture, in the absence of Matrigel or laminin/entactin enrichment, enables viable alveolosphere formation with high efficiency.

4. iAT2 Seeding Density Controls Alveolosphere Growth

Having shown that alveolospheres form in microwells, we used medium-size patterns to assess how iAT2 seeding density regulates growth and AT2 progeny within these engineered environments. Recent studies in intestinal organoids suggest a minimal number of cells are required to generate epithelial structures.[11] In addition, the initial aggregate size may induce paracrine signaling that directs self-assembly and growth of alveolospheres.[11] Thus, we seeded iAT2s at an average density of 15, 75, and 750 cells per individual microwell and monitored alveolospheres growth. At day 14, alveolospheres formed through all conditions (**Figure 3**A), which is consistent with the epithelial structures observed in 3D hydrogels (Figure 1). During the process of iAT2 self-assembly, alveolospheres grew in size as indicated by the increasing alveolosphere areas with culture with starting populations of 75 cells per well and higher, whereas lower seeding densities failed to generate growing alveolospheres (i.e., 15 cells, Figure 3B). Similar growth patterns were observed in smaller microwells, further supporting that alveolosphere assembly and growth depends on initial iAT2 seeding densities (Figure S9, Supporting Information).

The ability of iAT2s to generate alveolospheres is driven by their self-renewal potential and capacity to proliferate,[5] which may be influenced by the cell seeding density. EdU incorporation was used to visualize proliferating cells during the initial 7 days of culture (Figure 3C). While we observed proliferating iAT2s throughout all conditions, the percentage of EdU+ cells was increased for alveolospheres formed from higher cell seeding densities (Figure 3D). The increase in proliferative capacity further resulted in larger alveolospheres at day 7 (Figure 3E and Figure S10, Supporting Information), suggesting the influence of cell–cell contact and paracrine signaling. In addition, quantification of alveolosphere forming efficiency revealed that individual microwells retained 36 ± 14% of the alveolospheres with low cell seeding densities (15 cells), whereas greater efficiencies of 73 ± 21% to 98 ± 3% were maintained in microwells at higher seeding densities of 75 and 750 cells (Figure 3F).

We next sought to determine whether the microwell culture method supported AT2 progeny of alveolospheres, focusing on the fluorescent reporter and expression of surfactant protein C (pro-SFTPC), which is highly specific to AT2 cells.[16] At day 14, we observed $SFTPC^{GFP+}$ expressing cells in all alveolospheres that were also expressing pro-SFTPC, as identified by immunostaining (Figure 3G). Varying the initial cell seeding density had little influence on $SFTPC^{GFP+}$ levels, which ranged from 20% to 30%; however, lower cell seeding densities increased pro-SFTPC expression (Figure 3H). This is consistent with a previous study that altered iAT2 plating densities to enhance AT2 progeny within Matrigel,[15] and maintain more pure and high percentages of GFP+ cell populations.[5,17,18]

5. Microwell Hydrogels Maintain Alveolosphere Function

We next sought to define the cellular heterogeneity of alveolospheres and their AT2 progeny using single-cell RNA sequencing (scRNA-seq) and protein identification. To assess the functionality of microwell-cultured alveolospheres we used one condition (75 cells) and compared to Matrigel cultured alveolospheres. At 14 days, cells clustered into seven different clusters as visualized by uniform manifold approximation and projection (UMAP) and we identified several AT2-specific markers expressed by cells cultured under both conditions, including surfactant protein C (SFTPC) and surfactant protein B (SFTPB, **Figure 4**A), with little expression of off-target genes (Figure S11, Supporting Information). These data suggest that cells within alveolospheres similarly represent AT2-like cells.

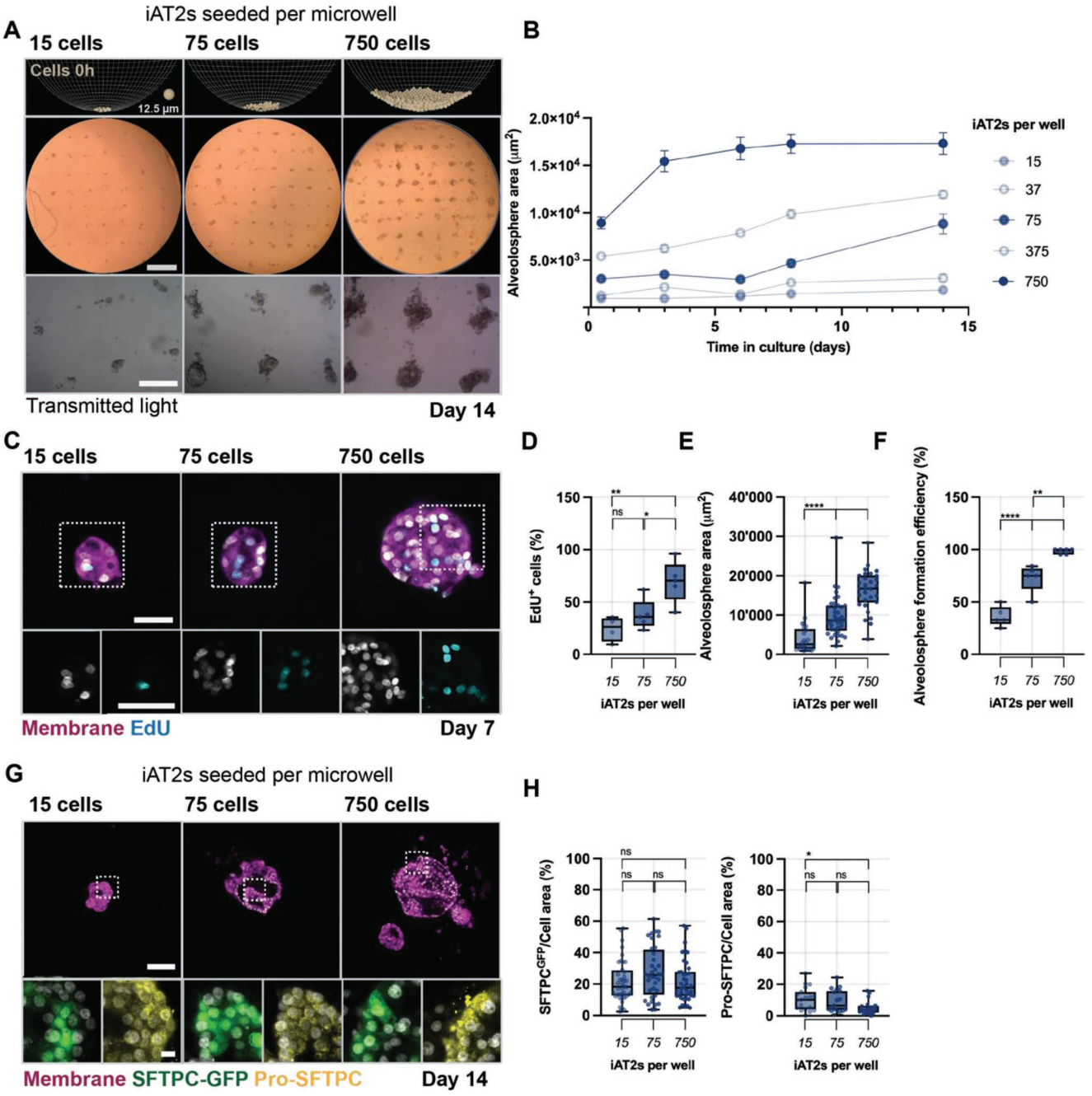

Figure 3. Effect of iAT2 seeding density on alveolosphere growth and fate. A) Simulation of iAT2 cell localization upon seeding (cross-section of center of microwell) and representative images of alveolospheres formed from 15, 75, and 750 iAT2s per individual medium size microwell (500 µm/200 µm width/depth) at 14 days of culture (scale bars: 1 mm (top) and 500 µm (bottom)). B) Time-course quantification of the projected area of alveolospheres formed from 15, 37, 75, 375, and 750 iAT2s over 14 days averaged from three independent experiments (see Figure S9, Supporting Information, for small-size microwells). C) Representative images of the incorporation of 5-ethynyl-2′-deoxyuridine (EDU) into alveolospheres over 7 days (cell mask membrane stain (magenta), nuclei (gray), and EdU (cyan), cell scale 12.5 µm (simulation), scale bars: 100 µm (inset 10 µm)). D) Quantification of the percentage of EdU^+ nuclei at 7 days in culture, averaged from four independent experiments ($*p < 0.05$, $**p < 0.01$, ns = not significantly different by ANOVA and Bonferroni's multiple comparisons test). E) Quantification of the area of alveolospheres at 14 days in culture ($****p < 0.0001$ by ANOVA and Bonferroni's multiple comparisons test, $n = 30$ (15 iAT2s), $n = 39$ (75 iAT2s), and $n = 31$ (750 iAT2s)). F) Quantification of the percentage of microwells containing alveolospheres at 14 days of culture, averaged from four independent experiments ($**p < 0.01$, $***p < 0.001$ by ANOVA and Bonferroni's multiple comparisons test). G) Representative images of $SFTPC^{GFP+}$ and Pro-SFTPC expression in alveolospheres at 14 days of culture (cell mask membrane stain (magenta), nuclei (gray), $SFTPC^{GFP+}$ (green), and pro-SFTPC (yellow), scale bars: 100 µm (inset 10 µm)). H) Quantification of $SFTPC^{GFP+}$ and pro-SFTPC expression per alveolosphere area (cell membrane stain) at 14 days ($*p < 0.05$, ns = not significantly different by ANOVA and Bonferroni's multiple comparisons test, $n = 40$ alveolospheres ($SFTPC^{GFP+}$), $n = 20$ alveolospheres (pro-SFTPC)).

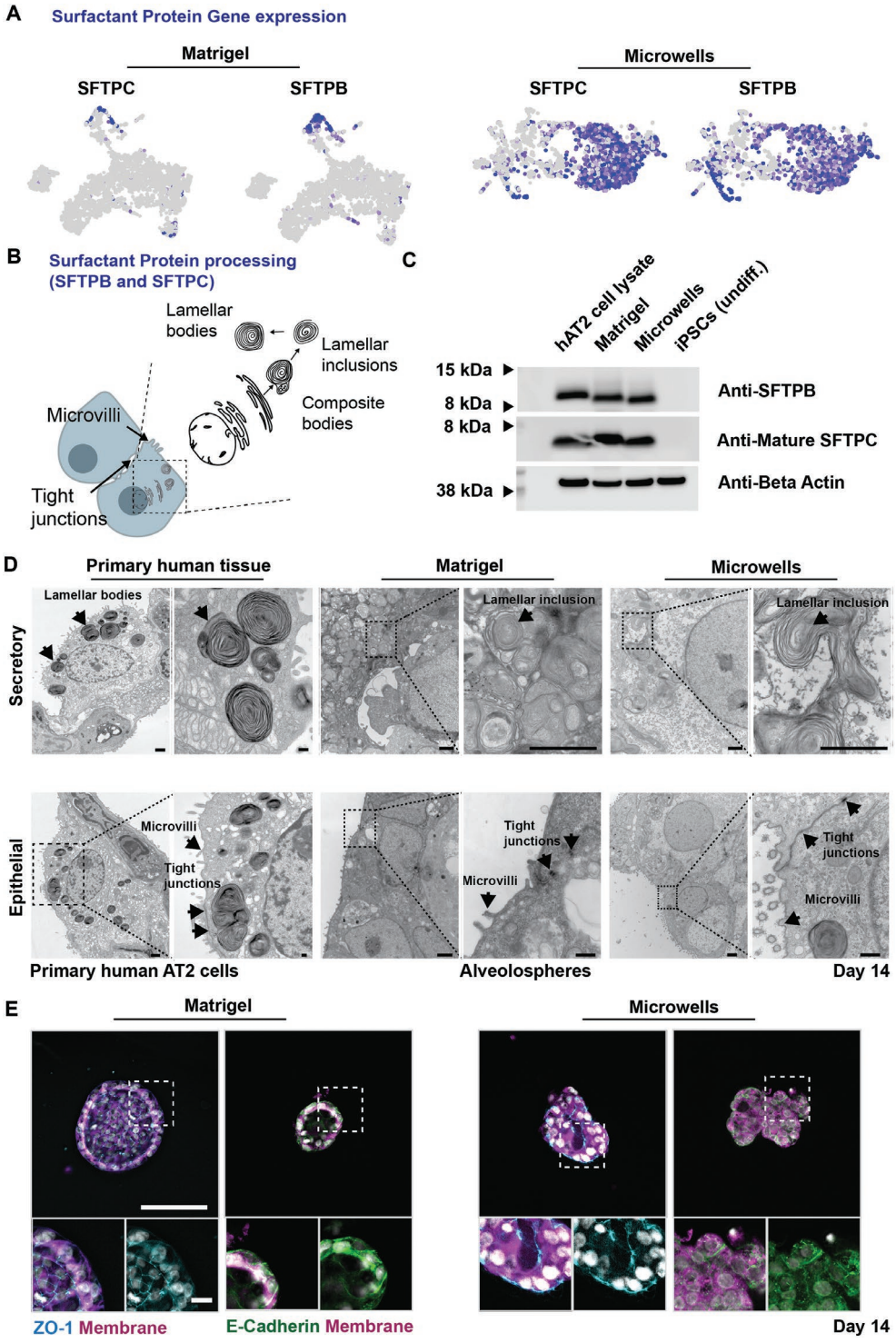

Figure 4. Characterization of microwell-cultured alveolospheres. A) UMAP representation of the expression of the AT2 markers surfactant protein C (SFTPC) and B (SFTPB) within alveolospheres at day 14 cultured in Matrigel and atop microwells. B) A schematic illustrating the ultrastructural characteristics of differentiated AT2 cells, including epithelial cell differentiation (cell contacts with neighboring cells through tight junctions at the apical part of the lateral cell membrane and microvilli on the apical cell membrane) and secretory differentiation (surfactant protein B (SFTPB) and surfactant protein C (SFTPC) storage organelles and lamellar bodies that are mature or still in the process of maturation, defined as lamellar inclusions). C) Western blot for SFTPB, mature SFTPC, and internal loading control beta-actin on human AT2 lysate, alveolospheres at day 14 cultured in Matrigel and atop microwells, as well as undifferentiated iPSCs. D) Representative TEM of AT2 cells from primary human lung tissue samples and alveolospheres at day 14 cultured in Matrigel and atop microwells (scale bars: 1 µm, inset 200 nm). E) Representative images of the tight junction marker ZO-1 in alveolospheres at day 14 cultured in Matrigel and atop microwells (cell mask membrane stain (magenta), nuclei (gray) and ZO-1 (cyan), scale bars: 100 µm (inset 10 µm). See Figure S12, Supporting Information, for additional images of ZO-1 and E-Cadherin expression).

Interestingly, a greater proportion of the total cells in microwell conditions maintained expression of mature AT2 markers, suggesting that microwell hydrogels may provide some advantages over Matrigel in terms of maintaining AT2 fate in alveolospheres.

In addition, previous studies showed that iAT2 cells in Matrigel exhibit some aspects of AT2 cell maturation including apical tight junctions, apical microvilli, and the expression of lamellar-like bodies[5] (Figure 4B). Therefore, we next assessed whether cells were able to process pro-SFTPs to mature SFTPB and SFTPC proteins that are exclusive to AT2 cells and essential components of surfactant.[16,19] As a comparison, proteins were also extracted from human primary AT2 cells, alveolospheres cultured in Matrigel, and undifferentiated iPSCs. Western blots immunostained with antibodies that recognize the fully mature 8 kDa form of SFTPB and SFTPC revealed production of mature forms of each protein. Primary human AT2 controls and cells from both Matrigel and microwell-cultured alveolospheres also expressed the mature 8 kDa SFTPB and SFTPC proteins, whereas no staining of undifferentiated iPSCs was detected (Figure 4C). As such, the microwell-cultured alveolospheres seem to efficiently process surfactant proteins into their mature form.

Next, we assessed whether the iAT2s in alveolospheres also formed lamellar bodies, the functional organelles in which surfactant is stored before exocytosis into the air spaces to form a phospholipid-rich film at the air–liquid interface.[19] Using transmission electron microscopy (TEM) analysis of primary human AT2 cells, these organelles are characterized by a tight packing of lipid lamellae into lamellar bodies. Similarly, Matrigel and microwell-cultured alveolospheres revealed lamellar body-like inclusions with a subset of inclusions expressing dense cores indicating the ongoing process of maturation (Figure 4D). Importantly, microwell-cultured alveolospheres further showed typical characteristics of epithelial differentiation, including the formation of tight junctions at the apical part of the lateral cell membrane and microvilli on the apical cell membrane (Figure 4D). These results suggest that alveolospheres when cultured in microwell hydrogels contain cells that form functional lamellar body-like inclusions, consistent with Matrigel cultures and findings reported in mature AT2 cells in vivo.[16,20] In addition, microwell-cultured alveolospheres had a polarized epithelium as the tight junction marker ZO-1 was expressed across the apical surface (Figure 4E) in addition to E-Cadherin, similar to Matrigel cultured alveolospheres (Figure S12, Supporting Information). While microwell hydrogel moduli had little influence on the expression of polarity markers, alveolosphere diameters decreased when cultured on stiffer hydrogel matrices (Figure S13, Supporting Information). Together, these findings demonstrate that microwell culture supports the development of an epithelial layer that resembles alveolospheres cultured in Matrigel.

6. Orthotopic Transplantation of Human Alveolar Progenitors into Murine Lungs

Having shown that microwell-cultured alveolospheres retain adult AT2 phenotypic markers in vitro, we next sought to assess their viability and differentiation capacity in vivo. Recent studies have shown orthotopic transplantation of lung epithelial cells into injured lungs as a functional tool to interrogate the responsiveness of cells to in vivo signaling cues.[17,21–24] Here, we used bleomycin-induced tissue injury, characterized by spatial AT2 cell loss within damaged regions[25] (Figure S14, Supporting Information). Immunodeficient nonobese diabetic (NOD) severe combined immunodeficiency (SCID) gamma (NSG) mice were injured with bleomycin at day 0, followed at day 10 by intranasal inhalation of alveolar progenitors derived from microwell and Matrigel-derived alveolospheres upon digestion (**Figure 5**A). Immunostaining of human-specific nuclear and mitochondrial markers at day 14 post-transplantation showed discrete clusters of human cells, predominantly at the border of damaged alveolar regions in each of the recipient mice ($n = 3$ per group). Human cell clusters appeared to adopt similarity to neighboring alveoli and retain at least some alveolar differentiation, as indicated by some cells being positive for pro-SFTPC (Figure 5B). Furthermore, staining for Ki67 expression revealed several proliferating cells that were located across the human cell clusters (Figure 5C). When analyzing cell clusters and percentage of Ki67+, we observed minimal differences between cells transplanted from alveolospheres cultured in Matrigel and microwells (Figure S15, Supporting Information). The lack of Keratin 5 expression in both conditions further confirmed that transplanted cells did not trans-differentiate into basal cells (Figure S16, Supporting Information). Although in contrast to recent findings on the differentiation of transplanted primary AT2 cells into basal cells,[23] the ability of cells to respond to the in vivo niche may depend on their origin (e.g., primary vs iPSC-derived), further highlighting the potential of the orthotopic transplantation assay to probe cell plasticity. We did not detect receptors for advanced glycation endproducts, suggesting minimal differentiation into type 1 alveolar epithelial cells. Explanations for the lack of differentiation could be that the in vitro culture conditions were not supportive of AT1 differentiation,[5] the early time points upon transplantation, or the incompatibility between murine and human growth factors/extracellular matrix components that are required for efficient AT1 fate adoption. These findings suggest that alveolospheres when cultured within engineered microwell hydrogels can retain their proliferative capacity upon transplantation into injured murine lungs, consistent with results in Matrigel and previous observations.[26] However, the lack of AT1 cells in both culture conditions as well as transcriptomic differences when compared to primary AT2 cells[5] indicates that further optimization is still required for future applications, including cell-based therapies and disease modeling studies.

7. Conclusion

We have designed a versatile Matrigel-free culture system to generate lung alveolospheres either when embedded within 3D hydrogels or seeded atop microwell hydrogels. Previous studies to engineer organoids within microwell hydrogels have focused on the development of intestinal, pancreatic, and cancer organoids,[11–13] but there has been little work to use engineered culture systems for lung organoids. Often, customized engineering

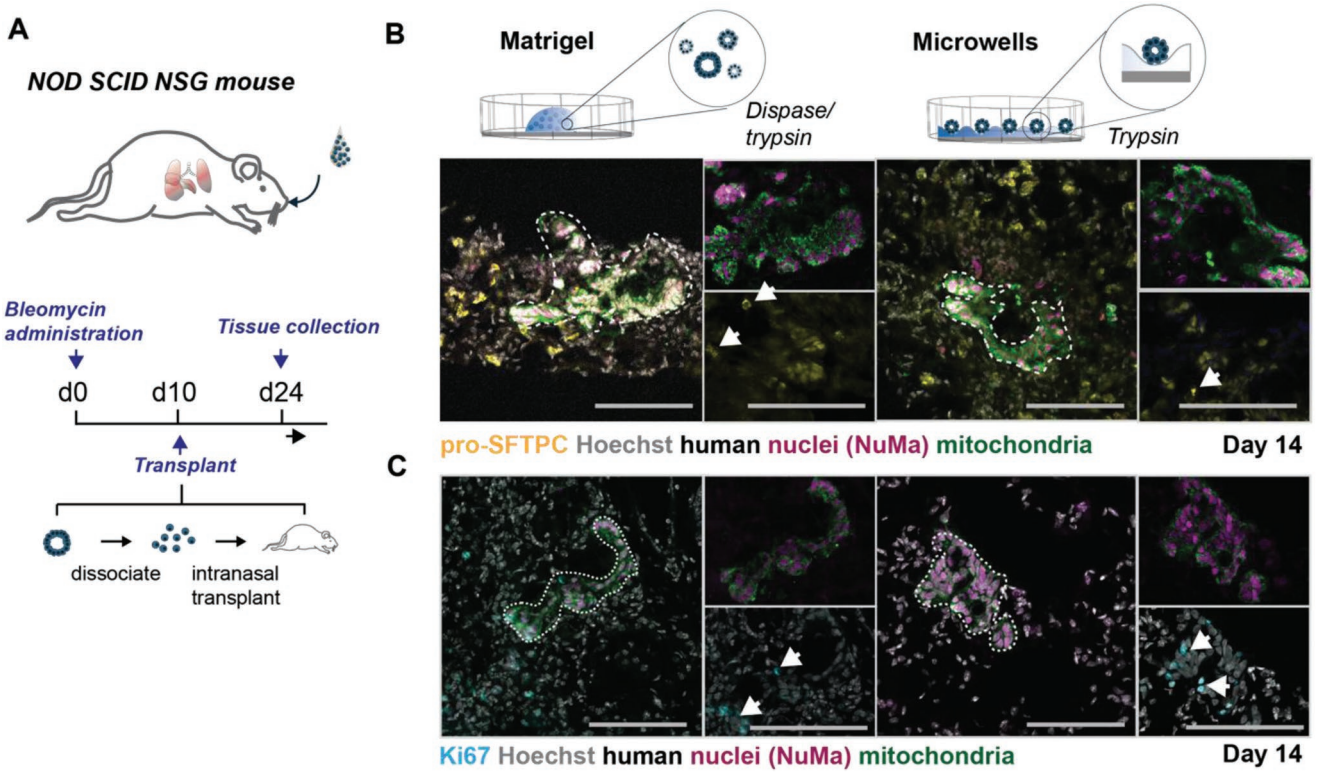

Figure 5. Applications of microwell-cultured alveolospheres. A) Schematic and transplant timeline of orthotopic transplantation of dissociated alveolospheres into bleomycin-injured, immunodeficient mouse lungs. B) Representative images of the survival of cells derived from alveolospheres upon culture in Matrigel or atop microwells (nuclei (gray), pro-SFTPC (yellow), human nuclear marker (magenta), and human mitochondrial marker (green), scale bars: 100 µm). See Figure S15 in the Supporting Information for quantification of the transplanted cell area. C) Representative images of the engraftment of cells derived from alveolospheres upon culture in Matrigel or atop microwells (nuclei (gray), Ki67 (cyan), human nuclear marker (magenta), and human mitochondrial marker (green), scale bars: 100 µm). See Figure S15 in the Supporting Information for quantification of percentage of $Ki67^+$ cells per transplanted cell area.

technologies or hydrogel chemistries are necessary to fabricate microwell hydrogels, which prevents their translation across groups. By using commercially available culture dishes with preformed microwells, we fabricated cytocompatible hydrogels with evenly spaced microcavities, which enabled the generation and culture of functional alveolospheres. Our data indicate that within microstructured hydrogels, human alveolospheres maintain their proliferative and differentiation capacity. One limitation of synthetic hydrogels as well as Matrigel constructs is the amount of background and noise, which lowers the image acquisition depth and quality. While this study focused on acquiring 3D images that maintain the original spatio-temporal information using confocal microscopy and computational clearing, paraffin-embedded or cryo-sectioned samples can be performed to improve image quality and resolution. We anticipate that by further modulating specific culture conditions such as hydrogel stiffness and composition, the microwell culture system can be used to study the role of cell-to-cell communication[27] and biophysical signaling during in vitro alveologenesis.

AT2 functionality was tested through analysis of surfactant protein processing and survival upon orthotopic transplantation of dissociated alveolospheres into lungs of immunocompromised mice. When microwell-cultured alveolospheres were transplanted into injured murine lungs, dissociated cells adopted alveoli-like structures while maintaining their proliferative capacity, and this was similar to alveolospheres formed within Matrigel. Previous work has reported data on the capacity of orthotopic transplanted epithelial progenitor cells to survive in injured murine lungs.[22–24] However, the technology described here could hold promise as a means to expand functional epithelial cells in Matrigel-free conditions for therapeutic applications. Further studies are required to probe whether cells are structurally and functionally integrated into mouse lungs, such as clonality and long-term replacement of injured epithelium; yet, to date, little is known regarding methods that confirm functional engraftment, or even the definition of engraftment in this context.[17] Although orthotopic transplantation assays are not yet sufficient to assess the contribution of transplanted cells to organ function, it provides a powerful platform to probe iPSC-derived lung epithelial cell viability, plasticity, and ability to incorporate into a compatible host tissue. Finally, although we observed lamellar inclusions and the functional capacity to process SFTPB and SFTPC to their mature form, extracted proteins from both conditions present relatively low amounts when compared to primary AT2 cells. While these differences might, in part, be explained by the effect of in vitro culture and sample processing, issues of limited characterization remain to be eliminated, further highlighting the need for culture platforms that support culture of both iPSC-based and primary AT2 cells.

Taken together, there are currently no strategies for the defined culture of lung alveolospheres in Matrigel-free conditions. Thus, the microwell hydrogels described herein provide means as an accessible culture system for the generation and maintenance of primary and iPSC-derived lung progenitors, which may be extendable to other epithelial progenitor and stem cell aggregates, as well as to various hydrogel types and compositions.

8. Experimental Section

Animals: The $R26R^{EYFP+}$ mouse line was purchased from Jackson Laboratories and the $Sftpc^{CreERT2}$ mouse line generously provided by Dr. Hal Chapman, and genotyping information was previously described.[28] All mice were maintained on a mixed background and were 3–5 weeks of age for experiments in this study. NOD.CgPrkdc^{scid} Il2rg^{tm1Wjl}/SzJ (NSG mice) were utilized as recipients for all transplantation experiments. Mice were 8–10 weeks old with male and female in equal proportions. Experiments were not blinded to mouse age or sex. All experiments were carried out under the guidelines set by the University of Pennsylvania's Institutional Animal Care and Use Committees and followed all NIH Office of Laboratory Animal Welfare regulations.

Bleomycin Lung Injury: 10 days prior cell transplantation, mice were first anesthetized using 3.5% isoflurane in 100% O_2 via an anesthesia vaporizer system. Mice were intranasally administered 4 mg kg^{-1} body weight bleomycin sulfate in a total volume of 30 µL phosphate-buffered saline (PBS). Only injured mice that lost ≈10% of their starting body weight by day 4 post injury and survived to the time of transplant were considered to be adequately injured and used for all transplantation experiments.

Orthotopic Cell Transplantation: Dissociated alveolospheres were administered via intranasal inhalation to NSG mice as previously described.[22] Recipients received 1.2 million iAT2 cells. Recipient mice were anesthetized with 3.5% isoflurane in 100% O_2 via an aesthesia vaporizer system and were intranasally administered cells by pipetting 30 µL single cell suspension in PBS (containing 1% penicillin–streptomycin) onto the nostrils of anesthetized mice visually confirmed by agonal breathing. All studies were approved by the University of Pennsylvania's Institutional Animal Care and Use Committees, protocol 806262, and followed all NIH Office of Laboratory Animal Welfare regulations.

Lung Tissue Harvest: Following sacrifice via isoflurane overdose, lungs were inflated at a constant pressure of 125 cm H_2O with 3.2% paraformaldehyde (PFA) for 30 min followed by incubation in 3.2% PFA for another 30 min at room temperature (RT). Fixed lungs were then washed in multiple PBS washed over the course of 1 h at RT, followed by an overnight incubation in 30% sucrose shaking at 4 °C, and then a 2 h incubation in 15% sucrose shaking at 4 °C, and then a 2 h incubation in 15% sucrose 50% Tissue-Tek O.C.T. compound at RT. Finally, fixed lungs were embedded in O.C.T. by flash freezing with dry ice and ethanol. 10 µm tissue sections were cut on a cryostat, followed by fixation in 4% PFA for 5 min, rinsed three times with PBS, and blocked in blocking solutions (PBS + 1% bovine serum albumin + 5% horse serum + 0.1% Triton X-100) for 45 min. Slides were incubated in primary antibodies in blocking solution overnight at 4 °C, washed three times with PBS + 0.1% Tween-20, and subsequently incubated with secondary antibodies for 2 h at RT. Slides were then washed with PBS Tween-20 prior to incubation in 1×10^{-6} M Hoechst. For hematoxylin and eosin (H&E) staining, lungs were prepared as described above and paraffin embedded using standard procedures.[29]

iPSC Cell Line Generation and Maintenance: All experiments using human iPSC lines were approved by the Institutional Review Board of the University of Pennsylvania. The human pluripotent stem cell line RUES2 was obtained from the University of Pennsylvania iPSC Core Facility. To generate a stable human-derived alveolar epithelial type II-like cells (iAT2) cell line, an EGFP cassette was knocked-in on one allele of the SFTPC gene (RUES2-SFTPC-EGFP) and differentiation performed as previously described.[15] Upon differentiation, iAT2 cells were passaged every 14 days and sorted for GFP+ cells using a BD FACSJazz cell sorter. GFP+ cells were plated as single cells using 90% Matrigel and a density of 400 cells μL^{-1}. Cells were cultured in Iscove's modified Dulbecco's medium (IMDM)/Ham's F12 media supplemented with 3 µg CHIR99021, 10 ng mL^{-1} KGF, 50×10^{-6} M dexamethasone, 0.1×10^{-3} M 3-isobutyl-1-methylxanthine (IBMX), 43 µg mL^{-1} 8-bromo-cAMP and primocin (CK+DCI medium), containing 10×10^{-6} M Y-27632 for the first 48 h after plating, followed by 5 days in K+DCI (without CHIR99021) and 7 days in CK+DCI. Alveolospheres were passaged every 14 days by digesting the Matrigel with 2 mg mL^{-1} dispase for 1 h at 37 °C, followed by incubation in 0.25% Trypsin/ethylenediaminetetraacetic acid for 10 min at 37 °C to obtain a single cell suspension. Cell quantification and viability were assessed using Trypan blue. Finally, cells were mixed with Matrigel, 50 µL drops formed within 24 well plates and incubated for 30 min at 37 °C and 5% CO_2.

Electron Microscopy: Alveolospheres were released from Matrigel using dispase or mechanically retrieved from microwells through several PBS washes, followed by fixation in 2.5% glutaraldehyde in 0.1% cacodylate buffer for at least 3 h at RT. Sample preparation was performed as recently reported.[5] Briefly, dehydration was performed with acetone on ice and graded ethanol series. Samples were then incubated in 100% acetone at RT for 2×10 min and in propylene oxide at RT for 2×15 min. Finally, samples were embedded in Embed-812 (Electron Microscopy Sciences), incubated in uranyl acetate and lead citrate and imaged with a JEOL 1010 electron microscope including a Hamamatsu digital camera (AMT Advantage image capture software).

Western Blotting: Western blots were performed to detect processed SFTPC and SFTPB protein as previously described.[30] Briefly, total protein content of cell lysates was assayed by the Bradford method followed by sodium dodecyl sulfate–polyacrylamide gel electrophoresis and immunoblotting. Western blotting used a previously published polyclonal pro-SFTPB antiserum ("PT3-SP-B" at 1:3000 dilution), a commercially available mature SFTPC antibody (WRAB-76694; Seven Hills Bioreagents at 1:2500 dilution), and Beta-Actin (Sigma Aldrich A1978 at 1:10 000 dilution) followed by an HRP-conjugated secondary antibody and visualization by enhanced chemiluminescence.

Hydrogel Preparation and Seeding: *Hydrogel Synthesis*: Norbornene-modified HA (NorHA) was synthesized as described previously.[31] The degree of modification was 26% by ^{1}H NMR (Figure S17, Supporting Information). Enzymatically (metalloproteinase (MMP)) degradable di-thiolated peptides (GCNSVPMSMRGGSNCG) and thiolated cell-adhesive RGD peptides (GCGYGRGDSPG) were purchased from Genscript. NorHA hydrogels were fabricated by thiol–ene addition crosslinking with either ultraviolet (microwells) or visible light (3D hydrogels) and the photoinitiator lithium phenyl-2,4,6-trimethylbenzoylphosphinate (LAP, Colorado Photopolymer Solutions).

iAT2 Encapsulation and Culture: Hydrogel precursor solutions (4 wt% polymer) were mixed with 1000 cells μL^{-1} (or as otherwise noted), 1×10^{-3} M thiolated RGD and mixed with or without laminin/entactin (Corning, 354259) or Matrigel at different concentrations, and photopolymerized with MMP-degradable peptide crosslinkers (400–500 nm, Omnicure S1500, Exfo) for 10 min at 10 mW cm^{-2}. Gels were crosslinked as 50 µL droplets atop thiolated coverslips and cultured in 48-well plates.[32] Cells were cultured in CK+DCI medium with 10 µg mL^{-1} Y27 for the first 48 h.

Microwell Fabrication and Culture: Microwell replicate topographies were fabricated by molding from cell culture surfaces (EZSPHERE) with different microwell width and depth. Briefly, poly(dimethylsiloxane) PDMS (Sylgard 184, Ellsworth Adhesives, 10:1 ratio) was mixed with Hexanes (30% vol/vol), and polymerized for 2 h at 80 °C. Hydrogel microwell topographies were fabricated through NorHA mixed with 1×10^{-3} M thiolated RGD and crosslinked with MMP-degradable peptide crosslinkers (320–390 nm, Omnicure S1500, Exfo) for 5 min at 5 mW cm^{-2}. The properties and fidelity of individual microwells and interspacing were maintained throughout the replication process (Figure S18, Supporting Information).

iPSC AT2 cells were added atop with different cell densities to enable seeding into individual microwells via gravity and cultured in CK+DCI medium (iAT2) or modified SAGM media as previously described.[29] Briefly, small airway epithelial cell growth basal media (SABM, Lonza) was mixed with insulin/transferrin, bovine pituitary extract, gentamycin, and retinoic acid as well as 0.1 mg mL^{-1} cholera toxin (Millipore Sigma), 25 ng mL^{-1} EGF (Peprotech), and 5% fetal bovine serum. CK+DCI and SAGM media were supplemented with 10 µg mL^{-1} Y27 for the first 48 h.

3D Rendering: To simulate initial cell seeding within microwells, Cinema 4D (C4D) rigid body dynamic simulations were used. Briefly, microwells were created according to various geometries and tagged as collider bodies, and cells (spheres, 12.5 µm) were tagged as rigid bodies and seeded into wells using simulated gravity. Cells were arrayed above the microwell with random seed points, and after settling, a Boole object was used to segment the simulation in half and rendering was carried out using C4D.

Image Acquisition: Bright-field images were acquired on a Laxco TM LMI-3000 Series Routine Inverted microscope with a 0.3MP USB 2.0 Color CMOS Digital Eyepiece Microscope Camera. Fluorescence images were taken on a Leica SP5 Confocal Microscope at 25 × 0.95 NA (water) and 63 × 1.4 NA (oil). Images in Figure 4E and Figure S11 in the Supporting Information were taken with an inverted Leica THUNDER Imager 3D Cell Culture System at 20 × 0.4 Corr (water) and a DFC9000 GT. Alveolospheres were randomly selected for all experiments and representative images shown in the manuscript without any selection criteria. For imaging, fixed and stained alveolospheres were mounted onto no.1 cover glass by flipping the coverglass-attached 3D hydrogel constructs or microwells up-side down. To measure alveolosphere area, circularity, and solidity, individual *z*-stacks were outlined manually using the freehand selection tool in ImageJ at three different *z*-locations to obtain an average per alveolosphere. Volume measurements of *z*-stacks were obtained using the 3D objects counter plugin in ImageJ. Sftpc reporter and protein expression were analyzed using the ImageJ thresholding function (Otsu). All measurements were performed blinded by at least two independent authors (C.L., V.B., or M.E.). 3D images obtained with the THUNDER system were processed using the Large Volume Computational Clearing (LVCC) settings as optimized by the system and 98% strength.

Single-Cell RNA Sequencing: To yield a sufficient number of cells, single cell suspensions from alveolospheres within 6 × 50 µL Matrigel droplets and 12x microwell hydrogels (8 mm diameter) were prepared as outlined above. Cells were pelleted and counted by trypan blue, resuspended in sterile PBS containing 0.04% bovine serum albumin for 10X Genomics, aiming for 10 000 cells. Cells were loaded onto a GemCode instrument (10x Genomics, Pleasanton, CA, USA) to generate single-cell barcoded droplets (GEMs) according to the manufacture's protocol. The resulting libraries were sequenced on an Illumina NovaSeq 6000 instrument.

Analysis of scRNA-seq Data: Reads were aligned and unique molecular identifier (UMI) counts were obtained using STAR-Solo (v2.7.9a).[33] Seurat (v4.0.1)[34] was used for all downstream scRNA-seq analysis. Cells with less than 200 genes, greater than 2 median absolute deviation above the median, and with potential stress signals of greater than 25% mitochondrial reads were removed. The read depth was 283 954 280 for the Matrigel sample and 270 398 732 for the microwell hydrogel sample. Data were normalized and scaled using the SCTransform function and adjusting for percent mitochondria, number of features per cell, and number of UMI per cell. Linear dimension reduction was done via principal component analysis (PCA), and the number of PCA dimensions was evaluated and selected based on assessment of an ElbowPlot. The uniform manifold projection (UMAP) data reduction algorithm was used to project the cells onto 2D coordinates. The Seurat function FeaturePlot was used to create the UMAP gene expression plots.

Statistical Analysis and Reproducibility: GraphPad Prism 9 software was used for statistical analyses. Statistical comparisons between two experimental groups were performed using two-tailed Student's *t*-tests and comparisons among more groups were performed using one-way or two-way analysis of variance (ANOVA) with Bonferroni post hoc testing. All experiments were repeated as described in the text.

Supporting Information

Supporting Information is available from the Wiley Online Library or from the author.

Acknowledgements

This work was supported by funding from the National Institutes of Health (K99HL151670 to C.L., F32DK117568 to M.D.D., R01HL145408 and U01HL152970 to M.F.B., K08HL150226 to J.B.K.), Department of Veterans Affairs (2I01BX001176 to M.F.B.), and National Science Foundation (NSF STC program (CMMI): 15-48571 to C.L., M.D.D., and J.A.B.). M.O. acknowledges funding by the German Research Federation (DFG, SFB 1449/B01). Florin Tuluc and staff at the Flow Cytometry Core Laboratory of Children's Hospital of Philadelphia, Biao Zuo and his staff at the Electron Microscopy Core at the University of Pennsylvania, the iPSCs core at the University of Pennsylvania for the RUES2 cell line, Luis Rodriguez for fruitful discussions, and Gargi Palashikar for assistance with lung harvest are thanked.

Conflict of Interest

The authors declare no conflict of interest.

Data Availability Statement

The data that support the findings of this study are available from the corresponding author upon reasonable request.

Keywords

biomaterials, hyaluronic acid, hydrogels, lung, organoids

Received: April 1, 2022
Revised: May 2, 2022
Published online: June 7, 2022

[1] a) M. Huch, J. A. Knoblich, M. P. Lutolf, A. Martinez-Arias, *Development* **2017**, *144*, 938; b) J. R. Spence, *Cell. Mol. Gastroenterol. Hepatol.* **2018**, *5*, 159.

[2] C. E. Barkauskas, M. I. Chung, B. Fioret, X. Gao, H. Katsura, B. L. Hogan, *Development* **2017**, *144*, 986.

[3] a) H. Surendran, S. Nandakumar, R. Pal, *Stem Cells Dev.* **2020**, *29*, 1365; b) J. Huang, A. J. Hume, K. M. Abo, R. B. Werder, C. Villacorta-Martin, K.-D. Alysandratos, M. L. Beermann, C. Simone-Roach, J. Lindstrom-Vautrin, J. Olejnik, E. L. Suder, E. Bullitt, A. Hinds, A. Sharma, M. Bosmann, R. Wang, F. Hawkins, E. J. Burks, M. Saeed, A. A. Wilson, E. Mühlberger, D. N. Kotton, *Cell Stem Cell* **2020**, *27*, 962; c) Y. Li, D. M. Renner, C. E. Comar, J. N. Whelan, H. M. Reyes, F. L. Cardenas-Diaz, R. Truitt, L. H. Tan, B. Dong, K. D. Alysandratos, J. Huang, J. N. Palmer, N. D. Adappa, M. A. Kohanski, D. N. Kotton, R. H. Silverman, W. Yang, E. E. Morrisey, N. A. Cohen, S. R. Weiss, *Proc. Natl. Acad. Sci. USA* **2021**, *118*, e2022643118.

[4] a) C. E. Barkauskas, M. J. Cronce, C. R. Rackley, E. J. Bowie, D. R. Keene, B. R. Stripp, S. H. Randell, P. W. Noble, B. L. Hogan, *J. Clin. Invest.* **2013**, *123*, 3025; b) J. R. Rock, X. Gao, Y. Xue, S. H. Randell, Y. Y. Kong, B. L. Hogan, *Cell Stem Cell* **2011**, *8*, 639.

[5] A. Jacob, M. Morley, F. Hawkins, K. B. McCauley, J. C. Jean, H. Heins, C. L. Na, T. E. Weaver, M. Vedaie, K. Hurley, A. Hinds, S. J. Russo, S. Kook, W. Zacharias, M. Ochs, K. Traber, L. J. Quinton, A. Crane, B. R. Davis, F. V. White, J. Wambach, J. A. Whitsett, F. S. Cole, E. E. Morrisey, S. H. Guttentag, M. F. Beers, D. N. Kotton, *Cell Stem Cell* **2017**, *21*, 472.
[6] a) J. Kim, B.-K. Koo, J. A. Knoblich, *Nat. Rev. Mol. Cell Biol.* **2020**, *21*, 571; b) K. Kretzschmar, H. Clevers, *Dev. Cell* **2016**, *38*, 590.
[7] M. Hofer, M. P. Lutolf, *Nat. Rev. Mater.* **2021**, *6*, 402.
[8] a) M. M. Capeling, M. Czerwinski, S. Huang, Y.-H. Tsai, A. Wu, M. S. Nagy, B. Juliar, N. Sundaram, Y. Song, W. M. Han, S. Takayama, E. Alsberg, A. J. Garcia, M. Helmrath, A. J. Putnam, J. R. Spence, *Stem Cell Rep.* **2019**, *12*, 381; b) R. Cruz-Acuna, M. Quiros, A. E. Farkas, P. H. Dedhia, S. Huang, D. Siuda, V. Garcia-Hernandez, A. J. Miller, J. R. Spence, A. Nusrat, A. J. Garcia, *Nat. Cell Biol.* **2017**, *19*, 1326; c) N. Gjorevski, N. Sachs, A. Manfrin, S. Giger, M. E. Bragina, P. Ordonez-Moran, H. Clevers, M. P. Lutolf, *Nature* **2016**, *539*, 560; d) N. Broguiere, L. Isenmann, C. Hirt, T. Ringel, S. Placzek, E. Cavalli, F. Ringnalda, L. Villiger, R. Zullig, R. Lehmann, G. Rogler, M. H. Heim, J. Schuler, M. Zenobi-Wong, G. Schwank, *Adv. Mater.* **2018**, *30*, 1801621.
[9] a) K. T. Lawlor, J. M. Vanslambrouck, J. W. Higgins, A. Chambon, K. Bishard, D. Arndt, P. X. Er, S. B. Wilson, S. E. Howden, K. S. Tan, F. Li, L. J. Hale, B. Shepherd, S. Pentoney, S. C. Presnell, A. E. Chen, M. H. Little, *Nat. Mater.* **2021**, *20*, 260; b) J. A. Brassard, M. Nikolaev, T. Hubscher, M. Hofer, M. P. Lutolf, *Nat. Mater.* **2021**, *20*, 22.
[10] a) B. Cakir, Y. Xiang, Y. Tanaka, M. H. Kural, M. Parent, Y.-J. Kang, K. Chapeton, B. Patterson, Y. Yuan, C.-S. He, M. S. B. Raredon, J. Dengelegi, K.-Y. Kim, P. Sun, M. Zhong, S. Lee, P. Patra, F. Hyder, L. E. Niklason, S.-H. Lee, Y.-S. Yoon, I.-H. Park, *Nat. Methods* **2019**, *16*, 1169; b) M. Kasendra, A. Tovaglieri, A. Sontheimer-Phelps, S. Jalili-Firoozinezhad, A. Bein, A. Chalkiadaki, W. Scholl, C. Zhang, H. Rickner, C. A. Richmond, H. Li, D. T. Breault, D. E. Ingber, *Sci. Rep.* **2018**, *8*, 2871.
[11] N. Brandenberg, S. Hoehnel, F. Kuttler, K. Homicsko, C. Ceroni, T. Ringel, N. Gjorevski, G. Schwank, G. Coukos, G. Turcatti, M. P. Lutolf, *Nat. Biomed. Eng.* **2020**, *4*, 863.
[12] A. D. Gracz, I. A. Williamson, K. C. Roche, M. J. Johnston, F. Wang, Y. Wang, P. J. Attayek, J. Balowski, X. F. Liu, R. J. Laurenza, L. T. Gaynor, C. E. Sims, J. A. Galanko, L. Li, N. L. Allbritton, S. T. Magness, *Nat. Cell Biol.* **2015**, *17*, 340.
[13] S. Wiedenmann, M. Breunig, J. Merkle, C. von Toerne, T. Georgiev, M. Moussus, L. Schulte, T. Seufferlein, M. Sterr, H. Lickert, S. E. Weissinger, P. Möller, S. M. Hauck, M. Hohwieler, A. Kleger, M. Meier, *Nat. Biomed. Eng.* **2021**, *5*, 897.
[14] K. B. McCauley, K.-D. Alysandratos, A. Jacob, F. Hawkins, I. S. Caballero, M. Vedaie, W. Yang, K. J. Slovik, M. Morley, G. Carraro, S. Kook, S. H. Guttentag, B. R. Stripp, E. E. Morrisey, D. N. Kotton, *Stem Cell Rep.* **2018**, *10*, 1579.
[15] A. Jacob, M. Vedaie, D. A. Roberts, D. C. Thomas, C. Villacorta-Martin, K. D. Alysandratos, F. Hawkins, D. N. Kotton, *Nat. Protoc.* **2019**, *14*, 3303.
[16] M. F. Beers, Y. Moodley, *Am. J. Respir. Cell Mol. Biol.* **2017**, *57*, 18.
[17] K. D. Alysandratos, M. J. Herriges, D. N. Kotton, *Annu. Rev. Physiol.* **2021**, *83*, 529.
[18] a) K. D. Alysandratos, S. J. Russo, A. Petcherski, E. P. Taddeo, R. Acín-Pérez, C. Villacorta-Martin, J. C. Jean, S. Mulugeta, L. R. Rodriguez, B. C. Blum, R. M. Hekman, O. T. Hix, K. Minakin, M. Vedaie, S. Kook, A. M. Tilston-Lunel, X. Varelas, J. A. Wambach, F. S. Cole, A. Hamvas, L. R. Young, M. Liesa, A. Emili, S. H. Guttentag, O. S. Shirihai, M. F. Beers, D. N. Kotton, *Cell Rep.* **2021**, *36*, 109636; b) K. Hurley, J. Ding, C. Villacorta-Martin, M. J. Herriges, A. Jacob, M. Vedaie, K. D. Alysandratos, Y. L. Sun, C. Lin, R. B. Werder, J. Huang, A. A. Wilson, A. Mithal, G. Mostoslavsky, I. Oglesby, I. S. Caballero, S. H. Guttentag, F. Ahangari, N. Kaminski, A. Rodriguez-Fraticelli, F. Camargo, Z. Bar-Joseph, D. N. Kotton, *Cell Stem Cell* **2020**, *26*, 593.
[19] J. Pérez-Gil, *Biochim. Biophys. Acta* **2008**, *1778*, 1676.
[20] a) F. Brasch, G. Johnen, A. Winn-Brasch, S. H. Guttentag, A. Schmiedl, N. Kapp, Y. Suzuki, K. M. Müller, J. Richter, S. Hawgood, M. Ochs, *Am. J. Respir. Cell Mol. Biol.* **2004**, *30*, 449; b) A. Korimilli, L. W. Gonzales, S. H. Guttentag, *J. Biol. Chem.* **2000**, *275*, 8672.
[21] A. E. Vaughan, A. N. Brumwell, Y. Xi, J. E. Gotts, D. G. Brownfield, B. Treutlein, K. Tan, V. Tan, F. C. Liu, M. R. Looney, M. A. Matthay, J. R. Rock, H. A. Chapman, *Nature* **2015**, *517*, 621.
[22] A. I. Weiner, S. R. Jackson, G. Zhao, K. K. Quansah, J. N. Farshchian, K. M. Neupauer, E. Q. Littauer, A. J. Paris, D. C. Liberti, G. Scott Worthen, E. E. Morrisey, A. E. Vaughan, *npj Regener. Med.* **2019**, *4*, 17.
[23] J. J. Kathiriya, C. Wang, M. Zhou, A. Brumwell, M. Cassandras, C. J. Le Saux, M. Cohen, K.-D. Alysandratos, B. Wang, P. Wolters, M. Matthay, D. N. Kotton, H. A. Chapman, T. Peng, *Nat. Cell Biol.* **2022**, *24*, 10.
[24] A. J. Miller, D. R. Hill, M. S. Nagy, Y. Aoki, B. R. Dye, A. M. Chin, S. Huang, F. Zhu, E. S. White, V. Lama, J. R. Spence, *Stem Cell Rep.* **2018**, *10*, 101.
[25] A. Moeller, K. Ask, D. Warburton, J. Gauldie, M. Kolb, *Int. J. Biochem. Cell Biol.* **2008**, *40*, 362.
[26] A. I. Weiner, R. Fernandez, G. Zhao, G. Palashikar, M. F. de Mello Costa, S. Adams, C. J. Lengner, F. B. Johnson, A. E. Vaughan, *bioRxiv* **2020**, 2020.06.14.149831.
[27] J. A. Zepp, W. J. Zacharias, D. B. Frank, C. A. Cavanaugh, S. Zhou, M. P. Morley, E. E. Morrisey, *Cell* **2017**, *170*, 1134.
[28] H. A. Chapman, X. Li, J. P. Alexander, A. Brumwell, W. Lorizio, K. Tan, A. Sonnenberg, Y. Wei, T. H. Vu, *J. Clin. Invest.* **2011**, *121*, 2855.
[29] D. C. Liberti, M. M. Kremp, W. A. Liberti 3rd, I. J. Penkala, S. Li, S. Zhou, E. E. Morrisey, *Cell Rep.* **2021**, *35*, 109092.
[30] J. Katzen, B. D. Wagner, A. Venosa, M. Kopp, Y. Tomer, S. J. Russo, A. C. Headen, M. C. Basil, J. M. Stark, S. Mulugeta, R. R. Deterding, M. F. Beers, *JCI Insight* **2019**, *4*, 126125.
[31] C. Loebel, R. L. Mauck, J. A. Burdick, *Nat. Mater.* **2019**, *18*, 883.
[32] W. M. Gramlich, I. L. Kim, J. A. Burdick, *Biomaterials* **2013**, *34*, 9803.
[33] A. Dobin, C. A. Davis, F. Schlesinger, J. Drenkow, C. Zaleski, S. Jha, P. Batut, M. Chaisson, T. R. Gingeras, *Bioinformatics* **2012**, *29*, 15.
[34] Y. Hao, S. Hao, E. Andersen-Nissen, W. M. Mauck 3rd, S. Zheng, A. Butler, M. J. Lee, A. J. Wilk, C. Darby, M. Zager, P. Hoffman, M. Stoeckius, E. Papalexi, E. P. Mimitou, J. Jain, A. Srivastava, T. Stuart, L. M. Fleming, B. Yeung, A. J. Rogers, J. M. McElrath, C. A. Blish, R. Gottardo, P. Smibert, R. Satija, *Cell* **2021**, *184*, 3573.